Determination of Edge Fracture Limit Strain for AHSS in the ISO-16630 Hole Expansion Test

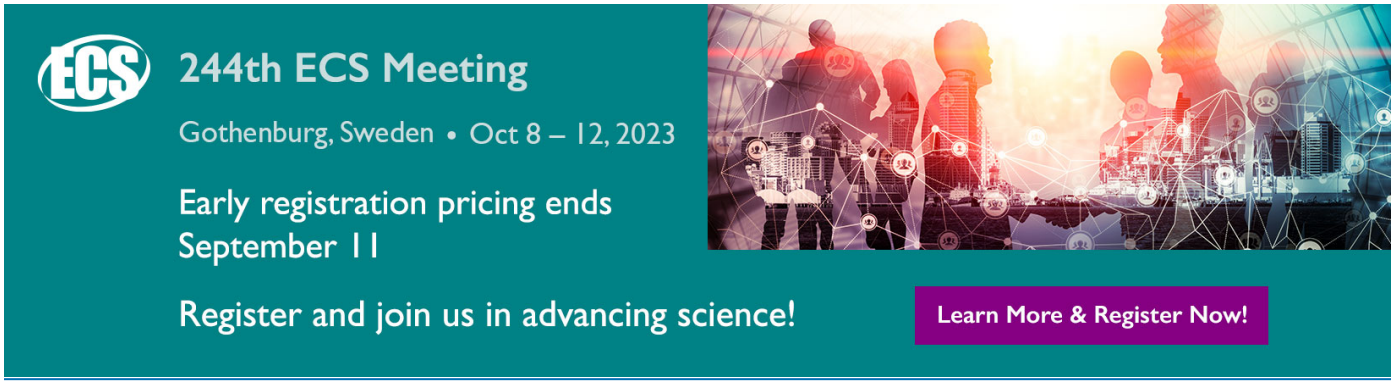

IOP Conf. Series: Materials Science and Engineering 1284 (2023) 012027 doi:10.1088/1757-899X/1284/1/012027

Determination of Edge Fracture Limit Strain for AHSS in the ISO-16630 Hole Expansion Test

A Barlo[1,*], M Sigvant[1,2], V Kesti[3], M S Islam[1], Q T Pham[1], J Pilthammar[1,2]

[1] Dept. of Mechanical Engineering, Blekinge Institute of Technology, Karlskrona, Sweden
[2] Volvo Cars Dept. 81110 Strategy Development, Olofström, Sweden
[3] SSAB Europe Oy, Raahe, Finland

E-mail: Alexander.Barlo@bth.se

Abstract. With the increased demand for application of sustainable materials and lightweight structures, the sheet metal forming industry is forced to push existing materials to the limits. One area where this is particular difficult is when it comes to assessing the formability limit for sheet edges. For decades, the ISO-16630 Hole Expansion Test (HET) has been the industry standard for expressing the edge formability of sheet metals through the Hole Expansion Ratio (HER). However, in recent years, this test has been criticized for its high scatter in results for repeated experiments. This scatter has been suspected to be caused by the operator-reliant post-processing of the test, or variations in the cutting conditions for the different test specimens. This study investigates the impact of shifting the evaluation point of the test from the through-thickness crack to the onset of surface failure on the reported scatter, as well as performs inverse modeling of the Hole Expansion Test to obtain an edge limit strain value.

1. Introduction

With the increased focus on the development and application of sustainable materials, the sheet metal forming industry faces more challenges than ever before. Demands for lightweight structures and complex component geometries forces the industry to push the capabilities of the materials to their limits, why it is more than ever important to be able to accurately determine failure limits for said materials.

One area where this historically has been difficult is on the topic of edge fracture. To describe the edge formability of sheet metals, the ISO standardized (ISO-16630) Hole Expansion Test (HET) [1] is most commonly used. This test has however over the years been heavily criticized for the high scatter in results and operator-reliant post-processing [2–5]. In an effort to reduce the reported scatter, Barlo et al [6] proposed a modification to the Hole Expansion Test setup to include draw beads (modified setup presented in Figure 1), thereby changing the boundary conditions of the test. In this study 63 repetitions of the Hole Expansion Test was performed off a DP800 AHSS material and yielded a mean Hole Expansion Ratio of $\overline{\lambda} = 31.184$ [%] with a standard deviation of $\sigma = 4.2910$. Even though the study did not succeed in reducing the reported scatter, it raised a valid question - when should the test be evaluated. In the ISO-standard, it is specified that the test should be evaluated at the time of appearance of a through-thickness crack, however, with the introduction of a 3D-DIC system in the modified setup, this opens up for evaluation at i.e. the onset of fracture, which aligns better with industrial needs.

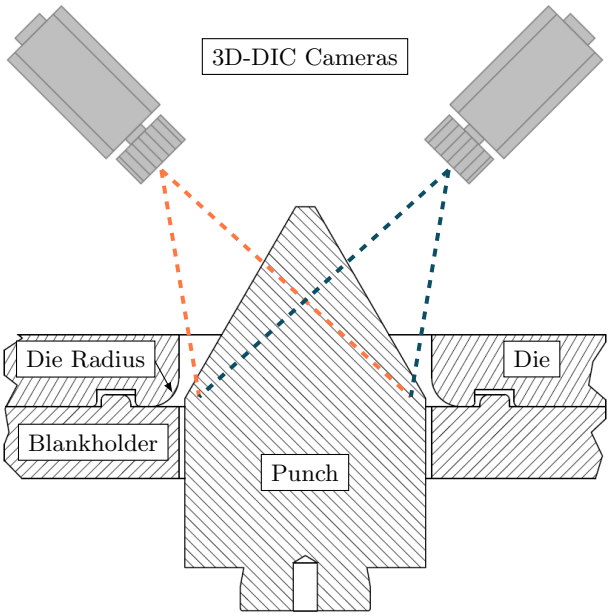

Figure 1. Modified experimental setup in fully closed configuration with draw beads and 3D DIC [6].

The application of the 3D-DIC system is however not as straight forward as usual. Due to the collar formation in the Hole Expansion Test, the DIC system fails to generate the strain field in the region of interest (RoI) around the hole edge. This is exemplified in Figure 2 where it is shown that the generated strain field does not cover the RoI. Therefore, this study will use the results from the 3D-DIC system to calibrate a Finite Element model for inverse modeling of the principal strains at the onset of edge fracture.

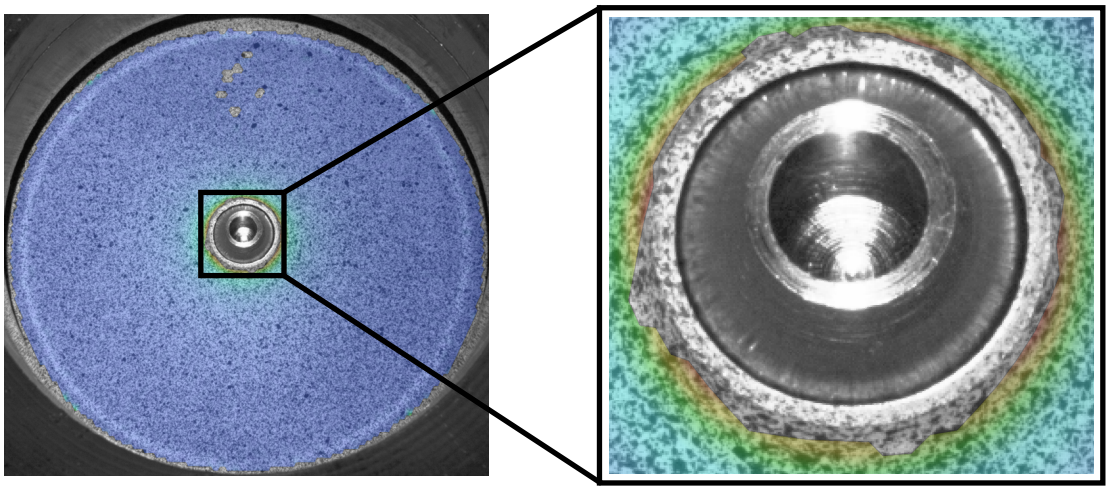

Figure 2. 3D-DIC strain field overlain experimental geometry with the RoI highlighted.

The number of experimental repetitions dealt with in this study is however significantly lower than the one presented in [6]. In this study, only 11 repetitions will be used (Test No. 10-20) as this test window shows a somewhat stable condition. In the original study, Test No. 5, 21, and

36 yielded no usable results as the test was terminated due to limitations by the test equipment, and from test 48 and onward, a downwards trend in results suspected to be caused by wear of the cutting tool, or changes in friction conditions between tool and blank. The selected range of results can be seen in Figure 3.

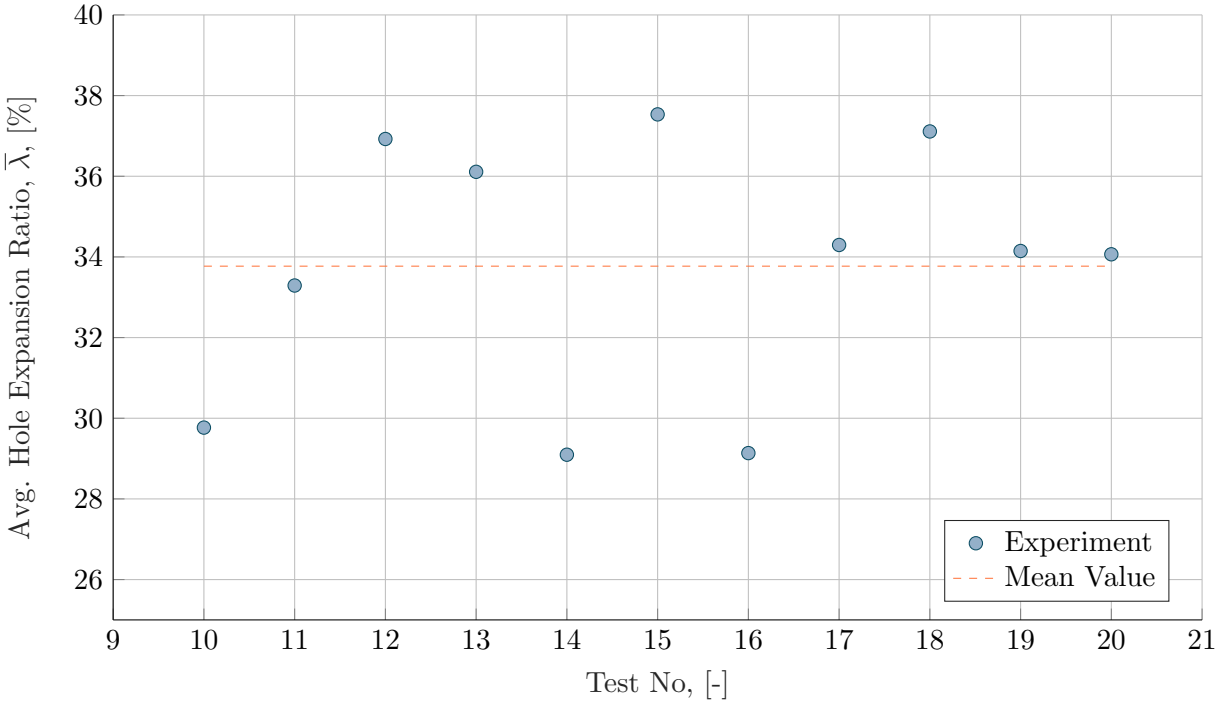

Figure 3. Results reported in [6] for test number 10-20. The test range has a mean Hole Expansion Ratio $\overline{\lambda} = 33.771$ [%] with at standard deviation of $\sigma = 3.175$.

2. Calibration of Finite Element Model

For the calibration of the Finite Element model, the commercial FE-code AutoForm™ R10 was used. For the description of the material behaviour, the BBC2005 material model was used, where the input parameters are presented in Table 1 and the hardening curve and yield surface can be found in Figure 4.

σ_0	σ_{45}	σ_{90}	σ_b	r_0	r_{45}	r_{90}	r_b	M
379.5	382.5	385.2	377.6	0.759	0.975	0.860	1.002	7.6

Table 1. Material parameters used as input to the BBC2005 material model in AutoForm™ R10. The exponent $M = 2k$ value has been obtained through inverse modeling to capture the principal strain predictions more accurately than with the standard values based on crystallographic structure [7].

For the modeling of the friction condition in the experimental setup, a combination of static Coulomb and dynamic TriboForm friction models were used. The dynamic TriboForm friction model was applied in the die radius (see Figure 1) where high tool pressures and sliding velocities were expected. The full friction model setup is outlined in Table 2.

For the exemplification of the calibration, the experimental results from Test No. 12 is used. For the setup of the model, an initial master element size of 32 [mm] with an allowed refinement

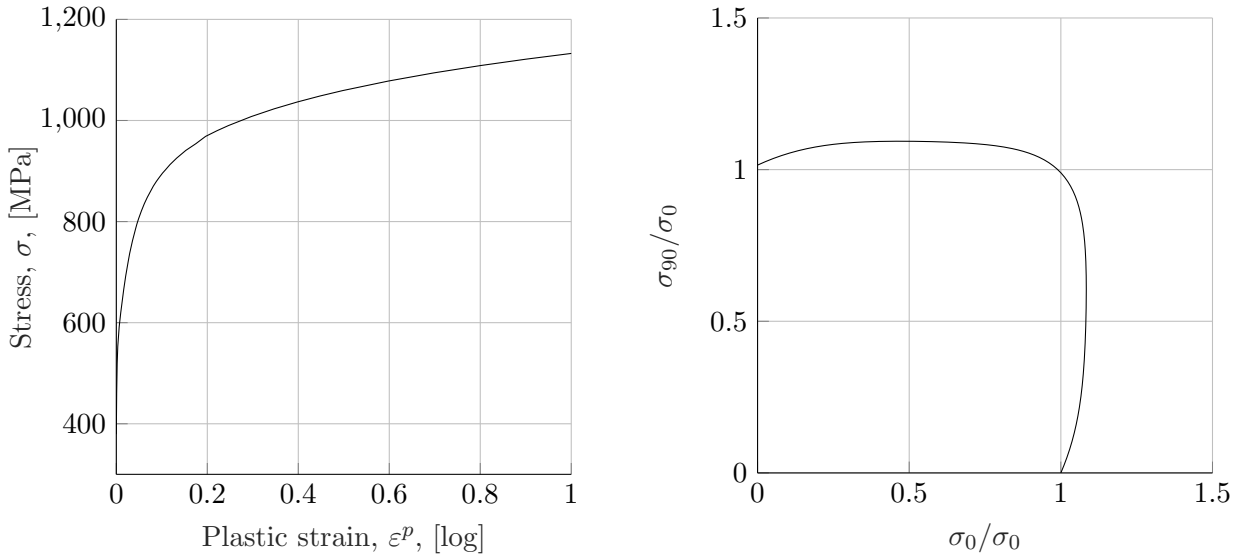

Figure 4. Hardening Curve and Yield Surface of the DP800 AHSS material.

Tool Part	**Friction Model**	**Friction Coefficient, μ, [-]**
Die	Coulomb	0.15
Binder	Coulomb	0.15
Punch	Coulomb	0.01
Die Radius	TriboForm	-

Table 2. Friction model setup of Finite Element Model.

level of 7 (allowing for an element size of 0.25 [mm]) was used. To avoid fusion and fission of elements in the RoI during the simulation, an initial refinement area (circular, radius 22.5 [mm]) was created with a constant element size of 0.5 [mm]. The initial and final mesh can be seen in Figure 5.

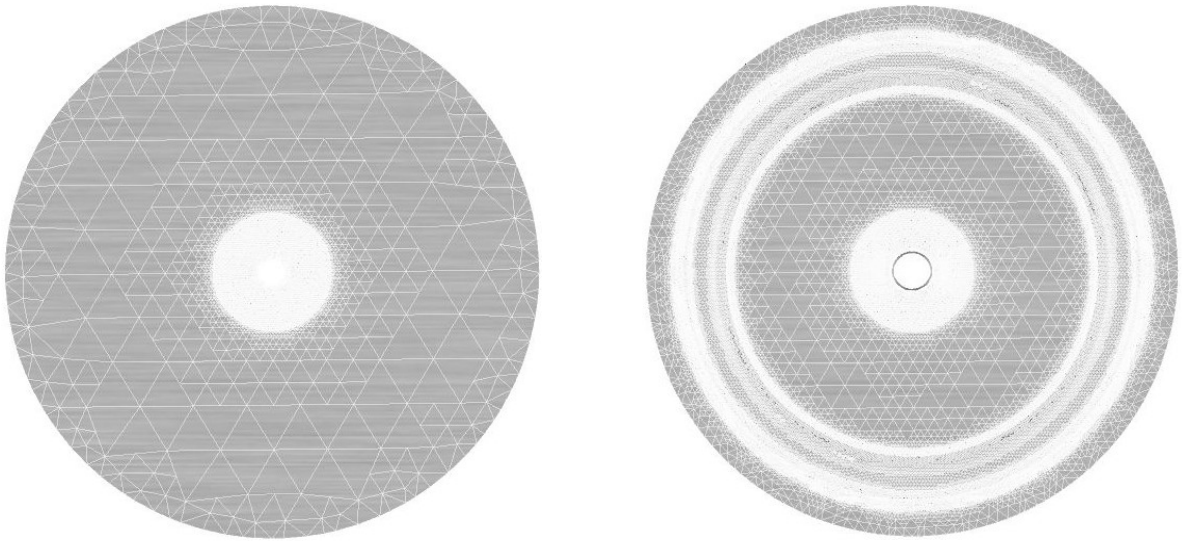

Figure 5. Initial and final mesh of the calibrated Finite Element model.

The Finite Element model is set up to dump data for every 0.5 [mm] punch displacement, why the results will be placed into these bins during evaluation. To check the accuracy of the model, initially the force-displacement response of the experiment and simulation was compared. This comparison can be found in Figure 6. As can be seen, there is a fairly good correspondence between the simulation and experiment except between roughly 6.5 and 8.5 [mm] of punch displacement. Here an unexpected decrease of forces is seen, that is assumed to be due to the numerical solution using more iterations before converging. The two markers in Figure 6 marking the failure illustrates how the simulated results are binned, where the difference in between simulation and experiment is approximately 0.2 [mm].

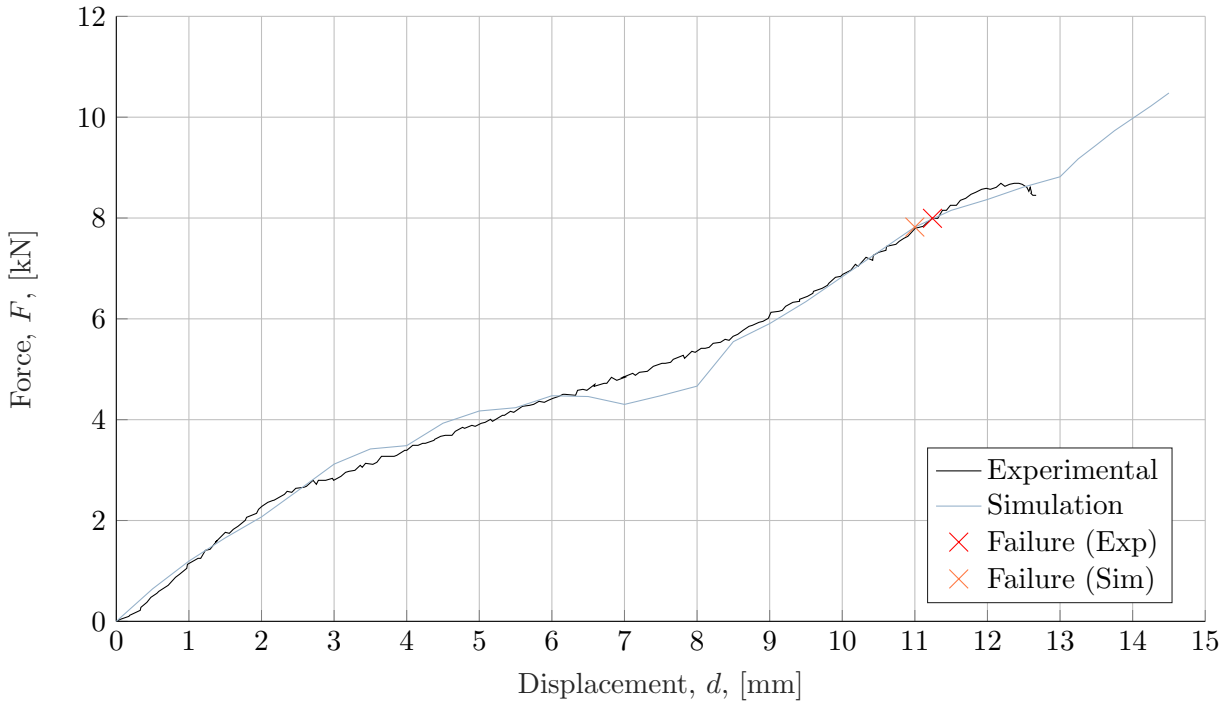

Figure 6. Comparison of experimental and simulated force-displacement response. The simulated failure is located approximately 0.2 [mm] before the experimental due to binning of results from the simulation.

Next, the deviation between the experimental and simulated geometries are checked. Two sections are created aligning with the x- and y-plane of the experimental measurements. The observed deviation along the two sections ranges between -0.1 and 0.32 [mm] in the Z-direction, yielding an acceptable geometrical fit between the experimental and simulated geometry. The section definition and deviation developments can be found in Figure 7.

Finally, the principal strain predictions from the simulation is compared to the experiment. For this, the sections defined in Figure 7 are used. It is expected that the maximum major and minor strain values will be significantly higher in the simulation due to the lack of information in the RoI in the measurement (see Figure 2), why the general development of the major and minor strains are of interest. Figure 8 presents the comparison of the principal strain. As can be seen, the principal strain profiles from the simulation matches the experimental quite well both for Section 1 and 2. As expected, the simulated maximum major strain is significantly higher than the experimental for both sections, indicating that the inverse modeling is justified.

With the calibration procedure presented, the 11 Hole Expansion Tests can be evaluated.

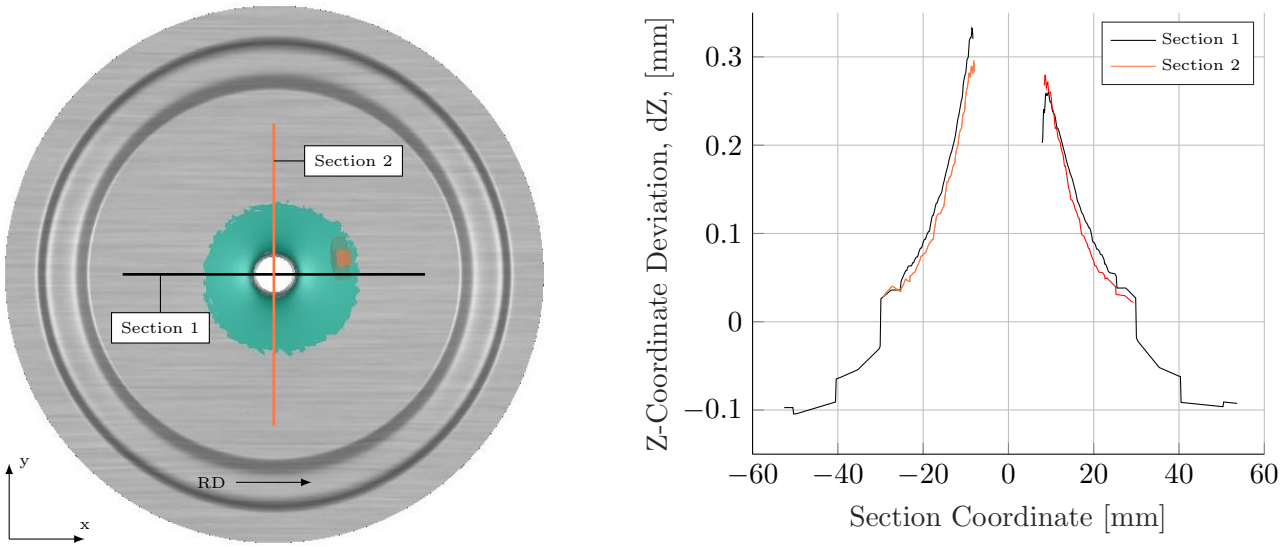

Figure 7. Z-coordinate deviation between experimental and simulated geometry across two sections.

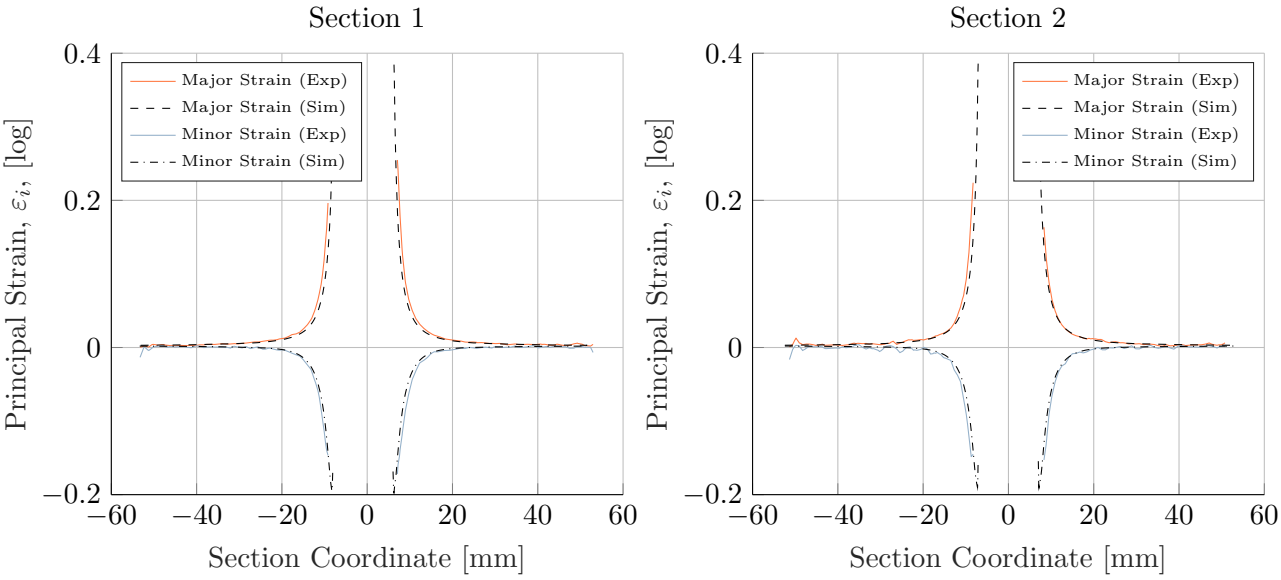

Figure 8. Comparison of principal strain profiles obtained from experiments and simulation for Section 1 and 2.

3. Results

With the shift of evaluation from through-thickness crack to the onset of surface fracture (illustrated in Figure 9), the impact of the crack propagation can now be investigated. Figure 10 presents the difference in punch depth for the 11 tests. As can be seen, there is variation between the change in punch displacement, indicating that the propagation of the crack through the surface could have an impact on the scatter of the determined Hole Expansion Ratios.

Using the calibrated FE-model, the failure strain can be identified for both the surface and membrane layer. Table 3 presents the identified punch displacement along with the maximum major strain (and the corresponding minor strain) for both the surface and membrane layer

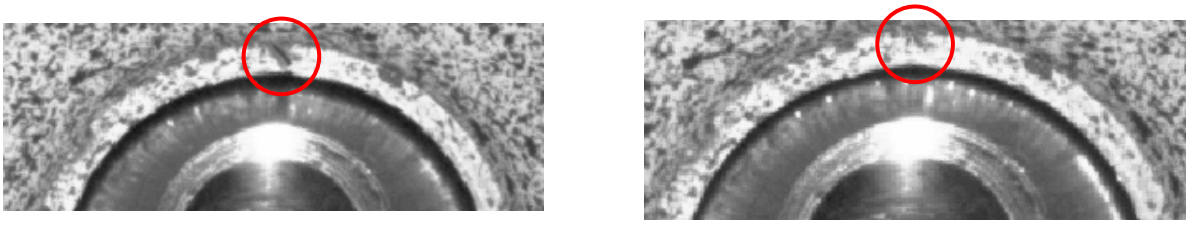

Figure 9. Illustration of the shift in evaluation point from through-thickness crack (left) to onset of surface crack (right).

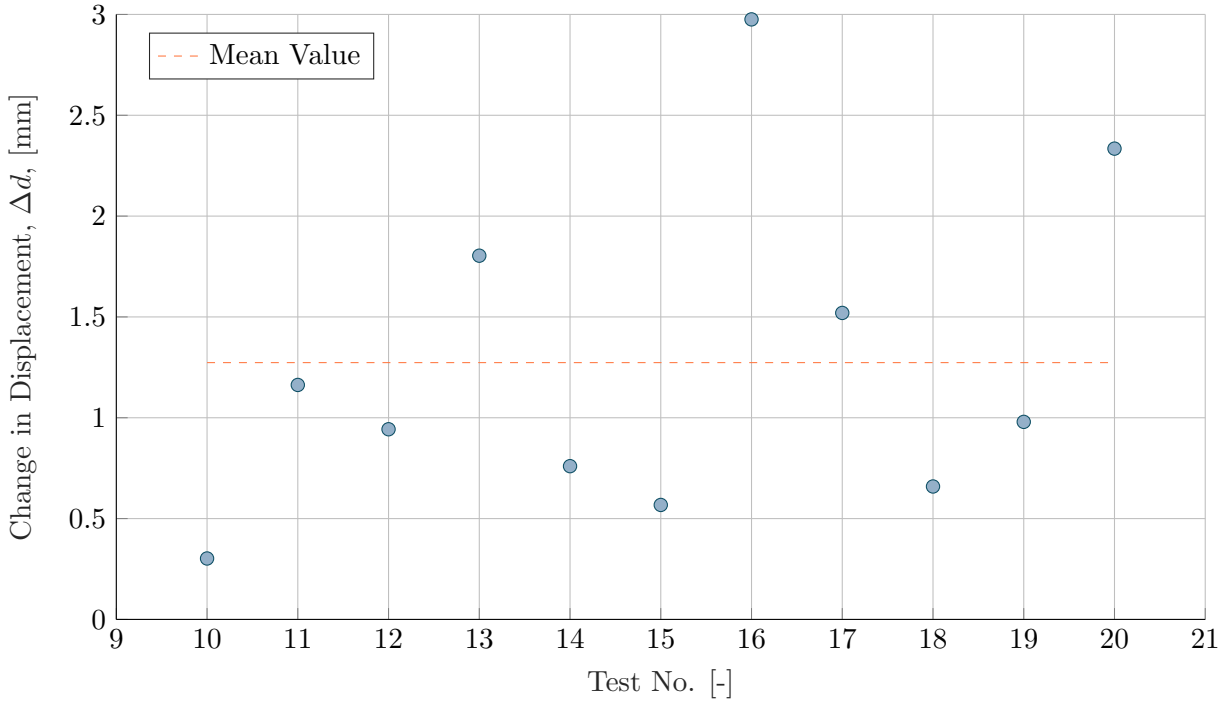

Figure 10. Difference in punch displacement between failure stages identified at through-thickness fracture [6] and onset of surface fracture. The differences have a mean value of 1.2734 [mm] with a standard deviation of $\sigma = 0.8158$

.

in the Finite Element model. As presented, the 11 tests investigated yielded seven different punch depths at the onset of surface fracture, with the failure strain at the surface layer ranging between 0.259 and 0.466, and the failure strain at the membrane layer ranging between 0.194 and 0.400.

Looking at the failure strains from a standard formability point of view, Figure 11 presents the seven failure bins at both the surface and membrane layer. Since the 11 experimental tests are divided into 'failure bins' the Forming Limit Diagram only presents the bins, why the number of occurrences of each bin can be found in Figure 12. It should here be noted that this figure presents the data for the surface layer, in terms of failure strain, but the number of occurrences are identical for the membrane layer.

		Surface Layer		Membrane Layer	
Test No	Displacement	Minor Strain	Major Strain	Minor Strain	Major Strain
10	11.0	-0.171	0.420	-0.096	0.356
11	10.5	-0.159	0.405	-0.085	0.332
12	11.0	-0.171	0.420	-0.096	0.356
13	10.0	-0.151	0.381	-0.075	0.308
14	10.0	-0.151	0.381	-0.075	0.308
15	12.0	-0.185	0.466	-0.116	0.400
16	7.5	-0.109	0.259	-0.040	0.194
17	10.0	-0.151	0.381	-0.075	0.308
18	11.5	-0.177	0.445	-0.107	0.380
19	10.5	-0.159	0.405	-0.085	0.332
20	9.5	-0.140	0.357	-0.071	0.285

Table 3. Identified failure strain points in surface and membrane layers for the 11 Hole Expansion Tests.

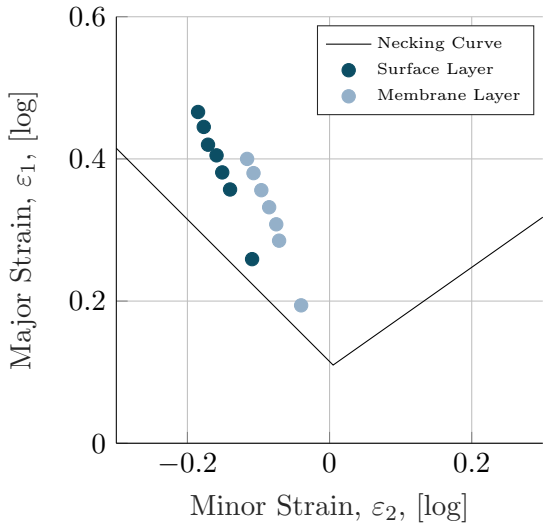

Figure 11. Failure points plotted against the necking curve for the DP800 material.

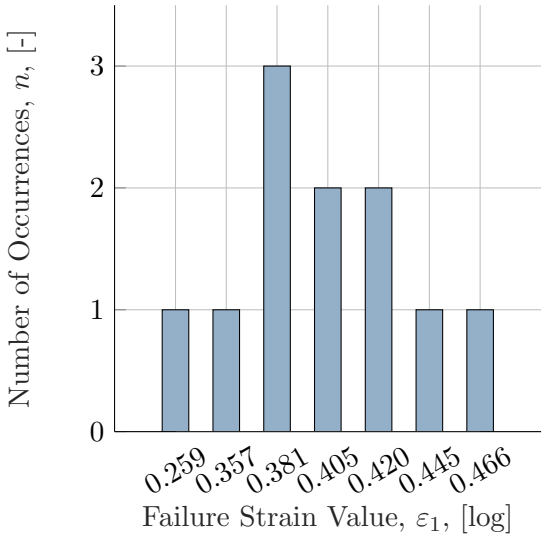

Figure 12. Number of occurrences for each failure strain for the surface layer.

4. Discussion

In the presented work 11 Hole Expansion Tests were analysed, and failure strain values were obtained through inverse Finite Element modeling. As presented in Table 3 and Figure 11 some degree of scatter in the result is still present. Interesting is the distribution of occurrences of the various failure strains presented in Figure 12, where a normal distribution is nearly obtained. It should here be noted, that since the binning is performed in intervals of 0.5 [mm] of punch displacement, small changes in displacement would move a result from one bin to another. In the case of the results from the tests with a failure strain of 0.381 at the surface level, the three tests are 0.3, 0.06, and 0.05 [mm] away from being placed in the next bin. If an assumption of normal distribution is made based on this, it could be an indication of some stochastic material behaviour contributing to the scatter in the test, however one should be aware of the low number of data points perhaps not being sufficient for the theoretical distribution of the sample mean to be distributed roughly normal [8]. Therefore, a more in-depth study, taking more samples

into account, should be performed to understand how e.g. how stochastic hardening influences simulation models.

5. Conclusion

The presented study attempted to eliminate the scatter in the ISO-16630 Hole Expansion Test by moving the point of evaluation from through-thickness crack to onset of surface fracture, along with identifying a failure limit strain through inverse Finite Element modeling. The study did not succeed in eliminating the scatter, but was able to obtain limit strain values from calibrated Finite Element Models. The study further uncovered a near normal distribution of failure strains for the 11 experimental tests investigated, indicating that stochastic material behaviour could contribute to the scatter in results.

Acknowledgements

Open Access funding was provided by Blekinge Institute of Technology. This study was also funded by VINNOVA in the Sustainable Production sub-program within Vehicle Strategic Research and Innovation (FFI) program (grant number 2020-02986).

References

[1] International Standard Organization 2018 Metallic Materials - sheet and strip - hole expanding test (ISO 16630).
[2] Schneider, M. *et al* 2015 Overview and comparison of various test methods to determine formability of a sheet metal cut-edge and approaches to the test results application in forming analysis *Mat.-wiss u. Werkstofftech* **46**(12) pp 1196-1217
[3] Larour P *et al* 2014 Evaluation of alternative stretch flangeability testing methods to iso 16630 standard *IDDRG 2014 Conference Proceedings, June 1-5, Paris, France.*
[4] Schneider, M. and U. Eggers 2011 Investigation on punched edge formability *IDDRG 2011 Conference Proceedings, June 5-8, Bilbao, Spain.*
[5] Hance B. M. 2017 Practical Application of the Hole Expansion Test *SAE Int. J. Engines* **10**(2)
[6] Barlo, A. *et al* 2022 A Study of the Boundary Conditions in the ISO-16630 Hole Expansion Test *IOP Conf. Ser.: Mater. Sci. Eng.* **1238**, p. 012031.
[7] Pilthammar, J. *et al.* 2018 BBC05 with non-integer exponent and ambiguities in nakajima yield surface calbration *Int. J. Mater. Form.* **14**, pp. 577-592.
[8] Ayyub, B. M. and R. H. McCuen 2011 Probability, statistics, and reliability for engineers and scientists *CRC Press*, 3rd edn.